

An Adolescent Mini-Neptune in the Kepler Field

L. G. BOUMA,¹ J. L. CURTIS,^{2,3} AND K. MASUDA⁴

¹*Department of Astrophysical Sciences, Princeton University, 4 Ivy Lane, Princeton, NJ 08540, USA*

²*Department of Astronomy, Columbia University, 550 West 120th Street, New York, NY 10027, USA*

³*Department of Astrophysics, American Museum of Natural History, New York, NY 10024, USA*

⁴*Department of Earth and Space Science, Osaka University, Osaka 560-0043, Japan*

(Received —; Revised —; Accepted —)

Submitted to Nature

ABSTRACT

Kepler 1627A is a G8V star previously found to host a $3.6 R_{\oplus}$ mini-Neptune on a 7.2 day orbit. The star was selected for observation by the Kepler satellite because it is nearby ($d \approx 333$ pc) and resembles the Sun. Combining data from Gaia with rotation periods from TESS, we show that Kepler 1627 is a member of the $35 \pm XX$ Myr old δ Lyr cluster. Kepler 1627Ab is therefore the youngest planet with a precise age found so far by the main Kepler mission. Analyzing the photometry, we find evidence that starspot crossings distort the average transit shape, and induce transit timing variations that suggest the planet is on a prograde orbit. The possibility that star-planet interactions could induce flares in the system is also explored. Future spectroscopic studies of Kepler 1627Ab may help clarify how the orbit and atmosphere of this mini-Neptune evolve. More generally, the combination of Gaia and TESS offers an opportunity to significantly expand the census of age-dated planets; we provide a literature concatenation of young stars to support this effort.

Keywords: planetary evolution (XXXX), stellar associations (1582), open star clusters (1160), stellar ages (1581),

1. MANUSCRIPT

While thousands of exoplanets have been discovered orbiting nearby stars, the vast majority of them are several billion years old. This makes it difficult to test theories for the origins of the different families of planets, since many expected evolutionary processes operate on timescales of less than 100 million years.

Corresponding author: L. G. Bouma
bouma.luke@gmail.com

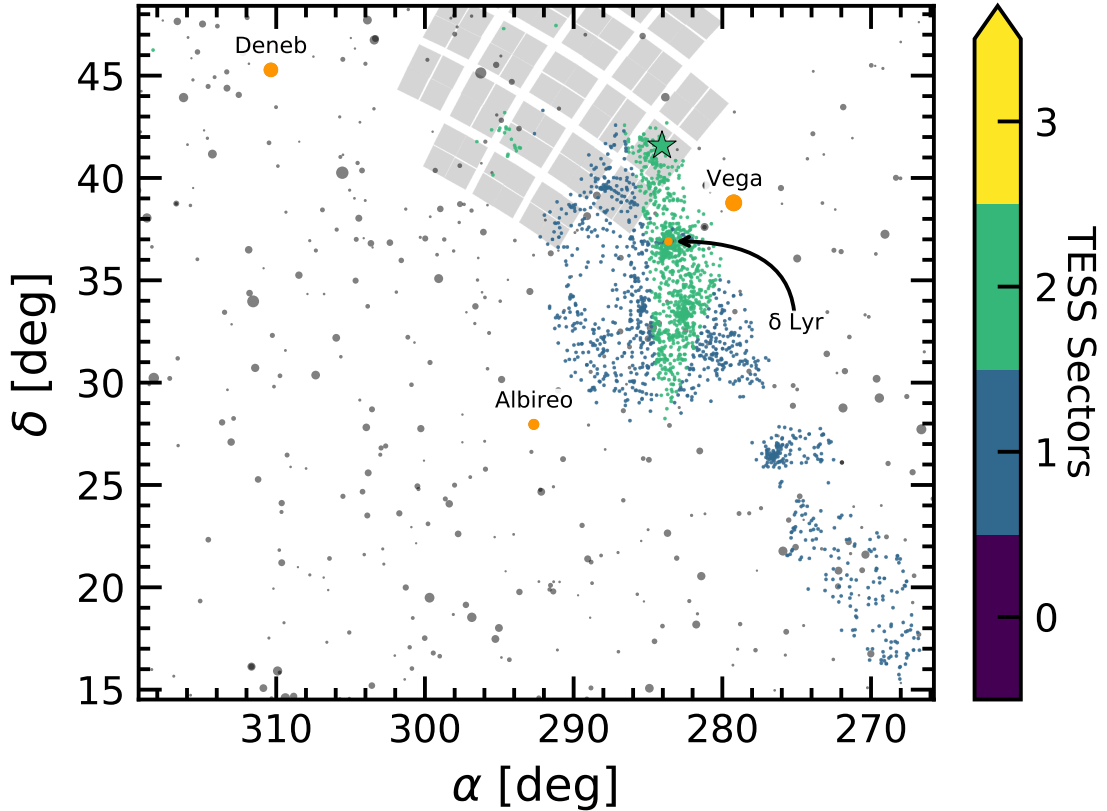


Figure 1. Kepler and TESS views of the δ Lyr cluster. Colored points are kinematically selected members of the δ Lyr cluster. Both Kepler (gray squares) and TESS (colored points) observed portions of the cluster. Naked-eye stars ($m_V < 6.5$) are shown in gray; four of them (orange points) have their names annotated. Kepler 1627 (green star) was observed during the entirety of the Kepler mission, and has been observed by TESS for two lunar months to date.

For instance, the “mini-Neptune” planets, thought to be made of molten rocky cores and extended atmospheric envelopes of hydrogen and helium, are expected to shrink in size by factors of several over their first 10^8 years (Owen 2020). Specifically, they start with sizes of $4\text{--}12 R_\oplus$ at the time of disk dispersal ($\lesssim 10^7$ years), and shrink to sizes of $2\text{--}4 R_\oplus$ by 10^8 years. This change is driven by a combination of stellar irradiation and internal heat that powers an outflow, which eventually depletes or entirely strips the envelope from the rocky core (Owen & Wu 2013; Gupta & Schlichting 2019). Discovering young planets and measuring their compositions and atmospheric outflows are key steps toward testing this paradigm, which is often invoked to explain the observed radius distribution of both mature exoplanets (Fulton et al. 2017), as well as younger planets (Bouma et al. 2020).

At the time of the main Kepler mission (2009–2013), only four open clusters were known in the Kepler field: NGC 6866, NGC 6811, NGC 6819, and NGC 6791, with ages spanning 0.7 Gyr to 9 Gyr (Meibom et al. 2011). Since that time, analyses of the kinematic, photometric, and astrometric Gaia data have expanded our knowledge of open cluster and moving group memberships (e.g., Cantat-Gaudin et al. 2018; Zari et al. 2018; Kounkel & Covey 2019; Meingast et al. 2021). As part of our Cluster Difference Imaging Photomet-

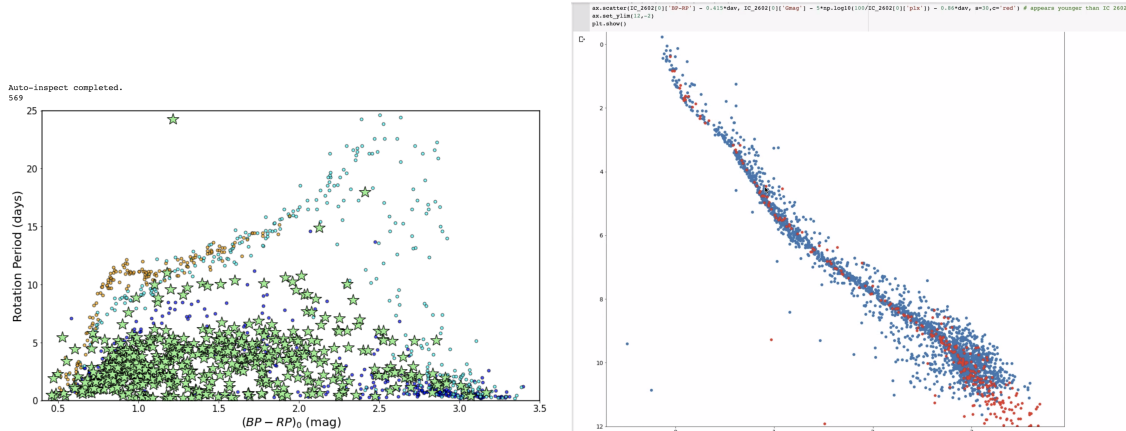


Figure 2. The δ Lyr cluster is 35 ± 15 Myr old. *Left:* TESS and Kepler rotations periods and dereddened Gaia colors, with the Pleiades (125 Myr; Rebull et al. 2016) and Praesepe (650 Myr; Douglas et al. 2017) shown for reference. Stars of a given color (mass) move up through time due to magnetic braking. The δ Lyr cluster has a 40 Myr gyrochronal age, as calibrated against the LDB-age of IC 2602. *Right:* HR diagram of the same comparison. **todo: caption improve.**

ric Survey (CDIPS, Bouma et al. 2019), we concatenated the available analyses from the literature, which yielded a list of candidate young and age-dated stars (see Section A).

Comparing our young star list against the Kepler field yielded two discoveries. The first, to be discussed in an upcoming analysis by J. Curtis et al., is that Kepler observed the ≈ 350 Myr open cluster Theia 520 (UBC 1). At least six Kepler planets are known in the cluster, including the Kepler-52 and Kepler-968 systems. The second discovery, and the focus of this work, is that Kepler observed a portion of the δ Lyr cluster, shown in Figure 1.

Kepler 1627 (KIC 6184894; KOI 5245; TIC 120105470) was previously reported to host a close-in mini-Neptune planet candidate, Kepler 1627Ab (Tenenbaum et al. 2012; Thompson et al. 2018). Given the planet's previous statistical validation by Morton et al. (2016), we decided to examine the age of the star and its cluster more closely. We collected the previously measured XXX Kepler rotation periods (CITEP MCQUILLAN2014), and measured YYY new stellar rotation periods for cluster members observed by TESS. We also performed an isochronal analysis. The results are shown in Figure 2. From the ensemble perspective, which provides the strongest constraints (SEE CITET SODERBLOM 2014), the age of the star is XX \pm YY Myr. Individual measurements of the star's rotation period and lithium abundance corroborate this conclusion.

If the Kepler 1627Ab transit signal is created by a bona fide planet, this age would make it the youngest planet yet found by the main Kepler mission¹. A portion of the light curve is shown in Figure ??, and the phase-folded transit is shown in Figure ?? . The dominant signal in the PDCSAP photometry is a quasi-period starspot signal with a peak-to-peak amplitude that varies between roughly 2% and 8%, depending on the degree of asymmetry in spot coverage between the stellar hemispheres. The starspot signal repeats every 2.642 ± 0.042 days, where we have adopted an uncertainty based on the scatter observed between

¹ The re-purposed K2 mission found two slightly younger systems: K2-33b (David et al. 2016; Mann et al. 2016) and V1298 Tau (David et al. 2019)

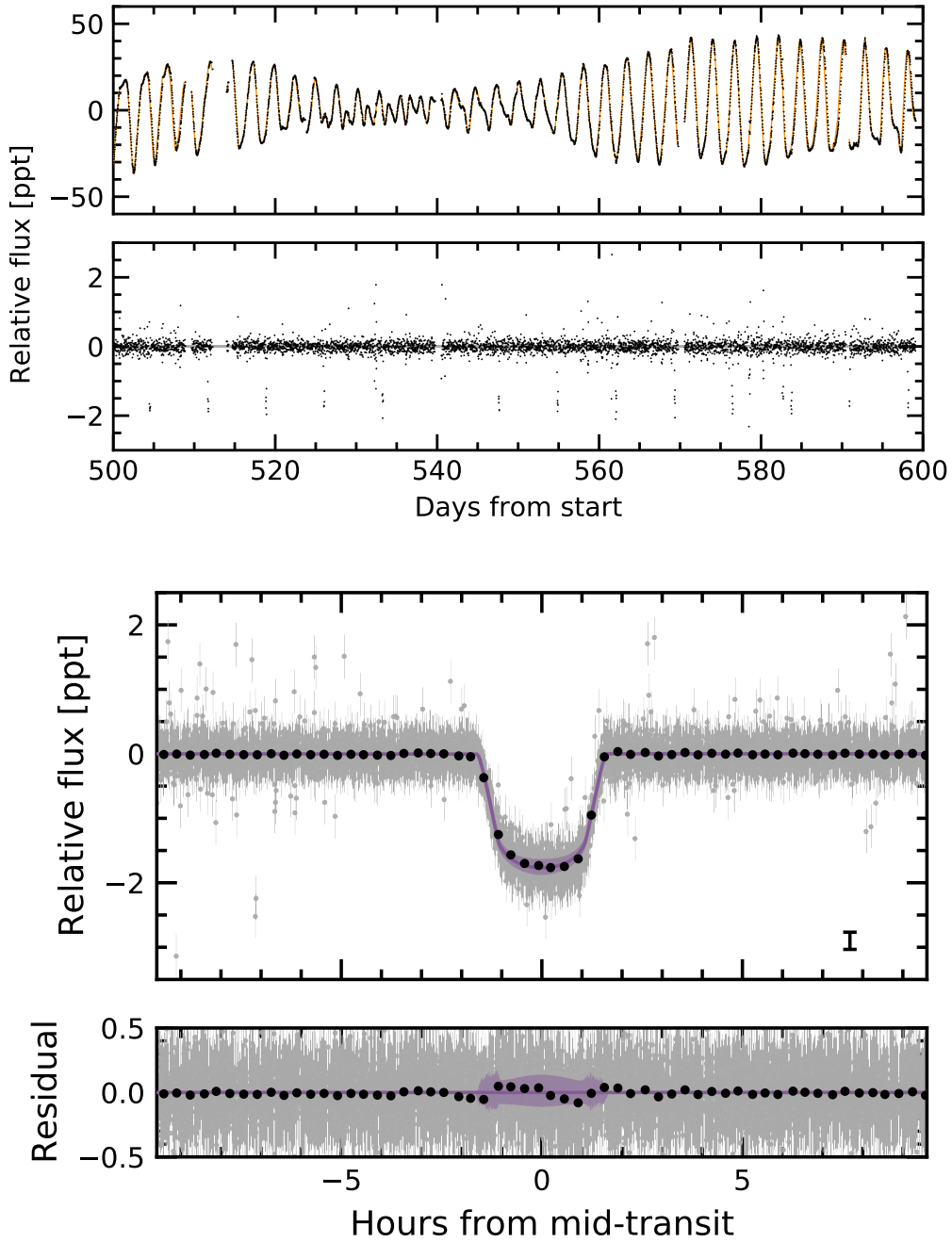


Figure 3. The light curve of Kepler 1627. *Top:* The full Kepler dataset spans 1,437 days (3.9 years), sampled at 30 minute cadence. A one hundred day segment is shown here. The *top panel* shows the PDCSAP median-subtracted flux in units of parts-per-thousand ($\times 10^{-3}$). The dominant signal is induced by starspots. The model for the stellar variability (orange line) is subtracted below, revealing the transits of Kepler 1627Ab, as well as other deviations from the stellar variability model. The Figure Set available online shows the entire 3.9 years of available data. *Bottom:* Phase-folded transit of Kepler 1627b, with stellar variability removed. The $2-\sigma$ model uncertainties and the maximum *a posteriori* model are shown as the faint purple band, and the dark purple line. Gray points are individual PDCSAP flux measurements; black points are binned to 20 minutes, with a representative error bar shown. The asymmetric residual visible during the transit is robust against detrending methods; we believe it is caused by starspot crossings.

different windows (quarters) of the time-series data. The details of how we model this starspot signal to derive the parameters of the planet are discussed in Section C. The results, given in Table 1, are consistent with a mini-Neptune sized planet ($3.56 \pm 0.04 R_{\oplus}$) on a circular 7.2 day orbit ($e < 0.XX$), around a G8V star ($0.91 \pm 0.05 R_{\odot}$). **TODO quote the eccentricity limit**

Could the transit signal be produced by anything other than a planet orbiting this near-solar analog? Morton et al. (2016) considered the false positive scenarios of a foreground eclipsing binary, a hierarchical triple-star binary system, and a background eclipsing binary. Based on the transit shape, Morton et al. (2016) found the latter scenario to be the only possible case, with a (model-dependent) probability of $\approx 10^{-5}$. While this statistical validation is reassuring, “validated” planets have been demonstrated to be false positives (Shporer et al. 2017). Most failures of the statistical validation approach arise when attempting to separate the smallest stars from identically-sized gas giant planets. With a size of $\approx 3.6 R_{\oplus}$, Kepler 1627b does not meet this concern. The fact that we detect a low-mass stellar companion in archival Keck-NIRC2 K_p-band (2.12 μ m) imaging does not change the conclusion: the companion contributes 1% of the flux observed by Kepler, which combined with the observed transit shape cannot be invoked as an explanation for the observed data (Section E).

Two additional new lines of evidence support the planetary interpretation. First, the ≈ 100 days of 1-minute short-cadence data enables a more precise measurement of the transit impact parameter: **todo numbers** it is constrained to be < 0.62 (3σ) from the 1-minute cadenced data, compared to $< 0.XX$ (3σ) from the 30-minute data. The second, and ultimately convincing line of evidence came from our transit timing analysis. **todo: Kento pls check numbers** We isolated each of the 144 observed transits to within ± 4.5 hr of each transit, and fitted each window with both *i*) a local second-order polynomial and transit, and *ii*) a local linear trend. We let the mid-time of each transit float, and then calculated the residual between the measured mid-time and that of a perfectly periodic orbit. This residual, the “transit timing variation” (TTV), is plotted in Figure 4 against the local linear slope. Only a handful of Kepler Objects of Interest have shown this correlation (Holczer et al. 2015), which is most readily interpreted as a TTV induced by unresolved starspot crossings (Mazeh et al. 2015). This is of course only possible if the planet is transiting the primary star, which excludes the any of the aforementioned false positive scenarios. It also implies that the planet’s orbit is prograde. The latter interpretation assumes that the dominant photometric variability is induced by dark spots, rather than bright faculae. Given the observed transition of Sun-like stellar variability from spot to faculae-dominated regimes, we expect this inference to be reasonably secure (Shapiro et al. 2016; Montet et al. 2017; Reinhold & Hekker 2020).

Kepler 1627Ab therefore provides a new extremum in the ages of the Kepler planets, and opens multiple avenues for study from the ground. Observations of its Doppler transit are expected to induce a Rossiter-McLaughlin anomaly with an amplitude of $\approx 20 \text{ m s}^{-1}$, and could yield a quantification of the stellar obliquity, and a means for verifying our transit-

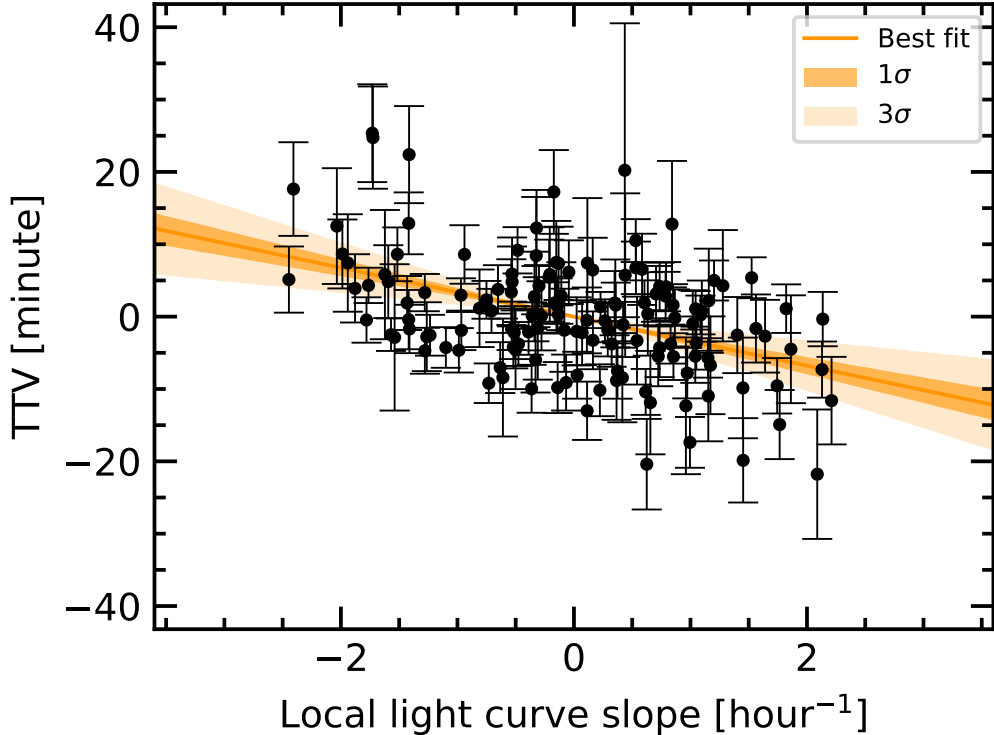


Figure 4. Evidence for a prograde orbit from transit timing variations. The time of each transit was measured, along with the local slope of the light curve. The two quantities appear anti-correlated, which is most easily explained by starspot crossings during the first (second) half of transit inducing a positive (negative) TTV, provided that the orbit is prograde (Mazeh et al. 2015).

timing based suggestion of a prograde orbit. Similar transit spectroscopy aimed at detecting either hydrogen or helium absorption could yield insight into the planet’s atmosphere, which is expected to be outflowing at a rate of $\mathbf{X.X} M_{\oplus} \text{yr}^{-1}$ (CITE). A more challenging measurement would be a measurement of the planet’s mass, through either detailed timing analyses of the Kepler data, or through a high-cadence multi-color radial velocity campaign. The mass would yield constraints on both the planet’s composition (“what is the extent of the initial gaseous envelope for a typical mini-Neptune?”), as well as its initial entropy (“hot” or “cold”? CITE).

The precision of the Kepler data itself may enable more detailed analyses without even needing to acquire more data. While our transit timing study did not yield the detection of any clearly significant planet-induced TTVs, the star’s flaring may be suggestive of star-planet interactions. Appendix D highlights an odd flare timing coincidence that may be worthy of further examination by those more knowledgeable than us.

Ultimately however, our age measurement for Kepler 1627Ab was enabled by identifying its connection to the δ Lyr cluster using the Gaia data. The Supplementary Table 2 enables similar crossmatches to already known planets, as well as forthcoming planets from the TESS mission (Ricker et al. 2015; Guerrero et al. 2021). An alternative approach also likely to bear fruit is to identify kinematic associations around exoplanet host stars using

Table 1. Priors and posteriors for the transit and stellar variability model fitted to the long-cadence Kepler 1627b photometric timeseries.

| Param. | Unit | Prior | Median | Mean | Std. Dev. | 3% | 97% | ESS | $\hat{R}-1$ |
|-----------------------|--------------------|---|------------|------------|-----------|-------------|-------------|--------------|-------------|
| <i>Sampled</i> | | | | | | | | | |
| P | d | $\mathcal{N}(7.20281; 0.01000)$ | 7.2028035 | 7.2028033 | 0.0000073 | 7.2027893 | 7.2028171 | 1910.5903732 | 0.0035905 |
| $t_0^{(1)}$ | d | $\mathcal{N}(120.79053; 0.02000)$ | 120.790504 | 120.790505 | 0.0009438 | 120.7886867 | 120.7922431 | 1564.1105056 | 0.0003213 |
| $\log R_p/R_\star$ | – | $\mathcal{U}(-4.605; 0.000)$ | -3.33523 | -3.33569 | 0.06618 | -3.45772 | -3.21617 | 1173.56574 | 0.00310 |
| b | – | $\mathcal{U}(0; 1+R_p/R_\star)$ | 0.3971 | 0.3886 | 0.2070 | 0.0204 | 0.7289 | 378.9528 | 0.0177 |
| u_1 | – | Kipping (2013) | 0.28 | 0.30 | 0.179 | 0.002 | 0.603 | 1161.95 | 0.005 |
| u_2 | – | Kipping (2013) | 0.425 | 0.381 | 0.314 | -0.197 | 0.912 | 900.884 | 0.002 |
| R_\star | R_\odot | $\mathcal{T}(0.910; 0.052)$ | 0.911 | 0.910 | 0.051 | 0.814 | 1.004 | 2265.830 | -0.001 |
| $\log g$ | cgs | $\mathcal{N}(4.600; 0.100)$ | 4.604 | 4.601 | 0.094 | 4.417 | 4.769 | 923.943 | 0. |
| $\langle f \rangle$ | – | $\mathcal{N}(0.500; 0.100)$ | 0.4999 | 0.4999 | 0.0003 | 0.4993 | 0.5005 | 2964.6676 | 0.0013 |
| $e^{(2)}$ | – | Van Eylen et al. (2019) | 0.127 | 0.168 | 0.147 | 0. | 0.446 | 518.492 | 0.004 |
| ω | rad | $\mathcal{U}(0.000; 6.283)$ | -0.235 | -0.170 | 1.867 | -2.879 | 3.132 | 1212.260 | 0.006 |
| $\log \sigma_f$ | – | $\mathcal{N}(\log \langle \sigma_f \rangle; 2.000)$ | -8.016 | -8.016 | 0.008 | -8.031 | -8.001 | 2224.427 | -0. |
| ρ | d | $\mathcal{U}(1.000; 10.000)$ | 2.953 | 2.955 | 0.096 | 2.777 | 3.131 | 1936.492 | 0. |
| σ | d^{-1} | InvGamma(1.000; 5.000) | 0.013 | 0.013 | 0.001 | 0.012 | 0.014 | 2155.687 | -0. |
| σ_{rot} | d^{-1} | InvGamma(1.000; 5.000) | 0.897 | 0.933 | 0.222 | 0.552 | 1.316 | 2147.324 | 0.003 |
| $\log P_{\text{rot}}$ | log(d) | $\mathcal{N}(0.958; 0.020)$ | 0.964 | 0.964 | 0.001 | 0.963 | 0.966 | 2486.029 | 0. |
| $\log Q_0$ | – | $\mathcal{N}(0.000; 2.000)$ | 12.935 | 12.960 | 0.454 | 12.157 | 13.857 | 2126.581 | 0.004 |
| $\log dQ$ | – | $\mathcal{N}(0.000; 2.000)$ | 0.029 | 0.021 | 2.032 | -3.785 | 3.780 | 1755.941 | 0. |
| f | – | $\mathcal{U}(0.100; 1.000)$ | 0.111 | 0.113 | 0.010 | 0.1 | 0.130 | 1253.358 | -0.0 |
| <i>Derived</i> | | | | | | | | | |
| R_p/R_\star | – | – | 0.036 | 0.036 | 0.002 | 0.031 | 0.040 | 1173.566 | 0.003 |
| ρ_\star | g cm^{-3} | – | 2.27 | 2.312 | 0.516 | 1.408 | 3.272 | 910.746 | 0.001 |
| R_p | R_{Jup} | – | 0.316 | 0.317 | 0.037 | 0.251 | 0.386 | 1692.736 | 0.001 |
| a/R_\star | – | – | 18.396 | 18.407 | 1.375 | 15.690 | 20.780 | 910.717 | 0.001 |
| $\cos i$ | – | – | 0.022 | 0.021 | 0.011 | 0.002 | 0.038 | 439.303 | 0.011 |
| T_{14} | hr | – | 2.822 | 2.823 | 0.057 | 2.710 | 2.917 | 1086.008 | 0.002 |
| T_{13} | hr | – | 2.578 | 2.566 | 0.083 | 2.430 | 2.714 | 590.630 | 0.011 |

NOTE— ESS refers to the number of effective samples. \hat{R} is the Gelman-Rubin convergence diagnostic. Logarithms through this table are in base- e . \mathcal{U} denotes a uniform distribution, \mathcal{N} a normal distribution, and \mathcal{T} a truncated normal bounded between zero and an upper limit much larger than the mean. (1) The ephemeris is in units of BJD-TDB - 2454833. (2) The eccentricity vectors are sampled in the $(e \cos \omega, e \sin \omega)$ basis.

the Gaia data, and to then verify these associations with ancillary rotation periods and spectroscopy (Tofflemire et al. 2021).

ACKNOWLEDGMENTS

L.G.B. and J.L.C. are grateful to T. David for help with the transit fitting, to R. Kerr for kindly providing us with the ? membership list prior to its publication, and to K. Ma-suda for advice on gravity darkening. L.G.B. acknowledges support by the TESS GI Program, programs G011103 and G022117, through NASA grants 80NSSC19K0386 and 80NSSC19K1728. L.G.B. was also supported by a Charlotte Elizabeth Procter Fellowship from Princeton University. This study was based in part on observations at Cerro Tololo Inter-American Observatory at NSF’s NOIRLab (NOIRLab Prop. ID 2020A-0146; 2020B-0029 PI: Bouma), which is managed by the Association of Universities for Re-

search in Astronomy (AURA) under a cooperative agreement with the National Science Foundation. This paper also includes data collected by the TESS mission, which are publicly available from the Mikulski Archive for Space Telescopes (MAST). Funding for the TESS mission is provided by NASA’s Science Mission directorate. We thank the TESS Architects (G. Ricker, R. Vanderspek, D. Latham, S. Seager, J. Jenkins) and the many TESS team members for their efforts to make the mission a continued success.

Software: astrobase (Bhatti et al. 2018), astropy (Astropy Collaboration et al. 2018), astroquery (Ginsburg et al. 2018), corner (Foreman-Mackey 2016), exoplanet (Foreman-Mackey et al. 2020), and its dependencies (Agol et al. 2020; Kipping 2013; Luger et al. 2019; Theano Development Team 2016), IPython (Pérez & Granger 2007), matplotlib (Hunter 2007), numpy (Walt et al. 2011), pandas (McKinney 2010), PyMC3 (Salvatier et al. 2016), scipy (Jones et al. 2001), TESS-point (Burke et al. 2020), wotan (Hippke et al. 2019).

Facilities: *Astrometry:* Gaia (Gaia Collaboration et al. 2018b, 2020). *Imaging:* Second Generation Digitized Sky Survey. *Spectroscopy:* CTIO1.5m (CHIRON; Tokovinin et al. 2013), AAT (HERMES; Lewis et al. 2002; Sheinis et al. 2015), VLT:Kueyen (FLAMES; Pasquini et al. 2002). *Photometry:* TESS (Ricker et al. 2015).

REFERENCES

- Agol, E., Luger, R., & Foreman-Mackey, D. 2020, *AJ*, **159**, 123
- Akeson, R. L., Chen, X., Ciardi, D., et al. 2013, *PASP*, **125**, 989
- Astropy Collaboration, Price-Whelan, A. M., Sipőcz, B. M., et al. 2018, *AJ*, **156**, 123
- Bhatti, W., Bouma, L. G., & Wallace, J. 2018, astrobase, <https://doi.org/10.5281/zenodo.1469822>
- Boisse, I., Pepe, F., Perrier, C., et al. 2012, *A&A*, **545**, A55
- Bouma, L. G., Hartman, J. D., Bhatti, W., Winn, J. N., & Bakos, G. Á. 2019, *ApJS*, **245**, 13
- Bouma, L. G., Hartman, J. D., Brahm, R., et al. 2020, *AJ*, **160**, 239
- Burke, C. J., Levine, A., Fausnaugh, M., et al. 2020, TESS-Point: High precision TESS pointing tool, Astrophysics Source Code Library, [ascl:2003.001](https://ascl.net/2003.001)
- Cantat-Gaudin, T., & Anders, F. 2020, *A&A*, **633**, A99
- Cantat-Gaudin, T., Jordi, C., Vallenari, A., et al. 2018, *A&A*, **618**, A93
- Cantat-Gaudin, T., Jordi, C., Vallenari, A., et al. 2018, *A&A*, **618**, A93
- Cantat-Gaudin, T., Jordi, C., Wright, N. J., et al. 2019, *A&A*, **626**, A17
- Cantat-Gaudin, T., Anders, F., Castro-Ginard, A., et al. 2020, *A&A*, **640**, A1
- Castro-Ginard, A., Jordi, C., Luri, X., et al. 2020, *A&A*, **635**, A45
- Cotten, T. H., & Song, I. 2016, *ApJS*, **225**, 15
- Damiani, F., Prisinzano, L., Pillitteri, I., Micela, G., & Sciortino, S. 2019, *A&A*, **623**, A112
- David, T., Hillenbrand, L., & Petigura, E. 2016, *Nature*, **534**, 658
- David, T. J., Petigura, E. A., Luger, R., et al. 2019, *ApJL*, **885**, L12
- Dias, W. S., Monteiro, H., Caetano, T. C., et al. 2014, *Astronomy and Astrophysics*, **564**, A79
- Douglas, S. T., Agüeros, M. A., Covey, K. R., & Kraus, A. 2017, *ApJ*, **842**, 83
- Esplin, T. L., & Luhman, K. L. 2019, *AJ*, **158**, 54
- Foreman-Mackey, D. 2016, *Journal of Open Source Software*, **1**, 24
- Foreman-Mackey, D., Czekala, I., Luger, R., et al. 2020, exoplanet-dev/exoplanet v0.2.6
- Fulton, B. J., Petigura, E. A., Howard, A. W., et al. 2017, *AJ*, **154**, 109
- Fürnkranz, V., Meingast, S., & Alves, J. 2019, *A&A*, **624**, L11
- Gagné, J., David, T. J., Mamajek, E. E., et al. 2020, *ApJ*, **903**, 96
- Gagné, J., & Faherty, J. K. 2018, *ApJ*, **862**, 138
- Gagné, J., Roy-Loubier, O., Faherty, J. K., Doyon, R., & Malo, L. 2018a, *ApJ*, **860**, 43
- Gagné, J., Mamajek, E. E., Malo, L., et al. 2018b, *ApJ*, **856**, 23
- Gaia Collaboration, Brown, A. G. A., Vallenari, A., et al. 2020, arXiv e-prints, arXiv:2012.01533
- Gaia Collaboration, Babusiaux, C., van Leeuwen, F., et al. 2018a, *A&A*, **616**, A10
- Gaia Collaboration, Brown, A. G. A., Vallenari, A., et al. 2018b, *A&A*, **616**, A1
- Ginsburg, A., Sipocz, B., Madhura Parikh, et al. 2018, Astropy/Astroquery: V0.3.7 Release
- Goldman, B., Röser, S., Schilbach, E., Moór, A. C., & Henning, T. 2018, *ApJ*, **868**, 32
- Guerrero, N. M., Seager, S., Huang, C. X., et al. 2021, arXiv:2103.12538 [astro-ph], arXiv: 2103.12538
- Gupta, A., & Schlichting, H. E. 2019, *MNRAS*, **487**, 24
- Hippke, M., David, T. J., Mulders, G. D., & Heller, R. 2019, *AJ*, **158**, 143
- Holczer, T., Shporer, A., Mazeh, T., et al. 2015, *ApJ*, **807**, 170
- Holczer, T., Mazeh, T., Nachmani, G., et al. 2016, *ApJS*, **225**, 9
- Hunter, J. D. 2007, Computing in Science & Engineering, **9**, 90
- Jones, E., Oliphant, T., Peterson, P., et al. 2001, Open source scientific tools for Python
- Kharchenko, N. V., Piskunov, A. E., Schilbach, E., Röser, S., & Scholz, R.-D. 2013, *A&A*, **558**, A53
- Kipping, D. M. 2013, *MNRAS*, **435**, 2152
- Kounkel, M., & Covey, K. 2019, *AJ*, **158**, 122
- Kounkel, M., & Covey, K. 2019, *AJ*, **158**, 122

- Kounkel, M., Covey, K., & Stassun, K. G. 2020, *AJ*, **160**, 279
- Kounkel, M., Covey, K., Suárez, G., et al. 2018, *AJ*, **156**, 84
- Kounkel, M., Covey, K., Suárez, G., et al. 2018, *AJ*, **156**, 84
- Kraus, A. L., Shkolnik, E. L., Allers, K. N., & Liu, M. C. 2014, *AJ*, **147**, 146
- Lewis, I. J., Cannon, R. D., Taylor, K., et al. 2002, *MNRAS*, **333**, 279
- Luger, R., Agol, E., Foreman-Mackey, D., et al. 2019, *AJ*, **157**, 64
- Mann, A. W., Newton, E. R., Rizzuto, A. C., et al. 2016, *AJ*, **152**, 61
- Mann, A. W., Johnson, M. C., Vanderburg, A., et al. 2020, *AJ*, **160**, 179
- Mazeh, T., Holczer, T., & Shporer, A. 2015, *ApJ*, **800**, 142
- McKinney, W. 2010, in Proceedings of the 9th Python in Science Conference, ed. S. van der Walt & J. Millman, 51
- Meibom, S., Barnes, S. A., Latham, D. W., et al. 2011, *The Astrophysical Journal Letters*, **733**, L9
- Meingast, S., & Alves, J. 2019, *A&A*, **621**, L3
- Meingast, S., Alves, J., & Rottensteiner, A. 2021, *A&A*, **645**, A84
- Montet, B. T., Tovar, G., & Foreman-Mackey, D. 2017, *ApJ*, **851**, 116
- Morris, B. M. 2020, *ApJ*, **893**, 67
- Morton, T. D., Bryson, S. T., Coughlin, J. L., et al. 2016, *ApJ*, **822**, 86
- Oh, S., Price-Whelan, A. M., Hogg, D. W., Morton, T. D., & Spergel, D. N. 2017, *AJ*, **153**, 257
- Owen, J. E. 2020, arXiv:2009.03919 [astro-ph], arXiv: 2009.03919
- Owen, J. E., & Wu, Y. 2013, *ApJ*, **775**, 105
- Pasquini, L., Avila, G., Blecha, A., et al. 2002, *The Messenger*, **110**, 1
- Pavlidou, T., Scholz, A., & Teixeira, P. S. 2021, *MNRAS*, **503**, 3232
- Pecaut, M. J., & Mamajek, E. E. 2013, *ApJS*, **208**, 9
- Pérez, F., & Granger, B. E. 2007, *Computing in Science and Engineering*, **9**, 21
- Plavchan, P., Barclay, T., Gagné, J., et al. 2020, *Nature*, **582**, 497
- Ratzenböck, S., Meingast, S., Alves, J., Möller, T., & Bomze, I. 2020, *A&A*, **639**, A64
- Rebull, L. M., Stauffer, J. R., Bouvier, J., et al. 2016, *AJ*, **152**, 113
- Reinhold, T., & Hekker, S. 2020, *A&A*, **635**, A43
- Ricker, G. R., Winn, J. N., Vanderspek, R., et al. 2015, *Journal of Astronomical Telescopes, Instruments, and Systems*, **1**, 014003
- Rizzuto, A. C., Mann, A. W., Vanderburg, A., Kraus, A. L., & Covey, K. R. 2017, *AJ*, **154**, 224
- Roccatagliata, V., Franciosini, E., Sacco, G. G., Randich, S., & Sicilia-Aguilar, A. 2020, *A&A*, **638**, A85
- Röser, S., & Schilbach, E. 2020, *A&A*, **638**, A9
- Salvatier, J., Wiecki, T. V., & Fonnesbeck, C. 2016, PyMC3: Python probabilistic programming framework
- Shapiro, A. I., Solanki, S. K., Krivova, N. A., Yeo, K. L., & Schmutz, W. K. 2016, *A&A*, **589**, A46
- Sheinis, A., Anguiano, B., Asplund, M., et al. 2015, *Journal of Astronomical Telescopes, Instruments, and Systems*, **1**, 035002
- Shporer, A., Zhou, G., Vanderburg, A., et al. 2017, *ApJL*, **847**, L18
- Tenenbaum, P., Christiansen, J. L., Jenkins, J. M., et al. 2012, *ApJS*, **199**, 24
- Theano Development Team. 2016, arXiv e-prints, abs/1605.02688
- Thompson, S. E., Coughlin, J. L., Hoffman, K., et al. 2018, *ApJS*, **235**, 38
- Tian, H.-J. 2020, *ApJ*, **904**, 196
- Tofflemire, B. M., Rizzuto, A. C., Newton, E. R., et al. 2021, *AJ*, **161**, 171
- Tokovinin, A., Fischer, D. A., Bonati, M., et al. 2013, *PASP*, **125**, 1336
- Ujjwal, K., Kartha, S. S., Mathew, B., Manoj, P., & Narang, M. 2020, *AJ*, **159**, 166
- Van Eylen, V., Albrecht, S., Huang, X., et al. 2019, *AJ*, **157**, 61
- Villa Vélez, J. A., Brown, A. G. A., & Kenworthy, M. A. 2018, *Research Notes of the American Astronomical Society*, **2**, 58

- Walt, S. v. d., Colbert, S. C., & Varoquaux, G.
2011, Computing in Science &
Engineering, 13, 22
- Wenger, M., Ochsenbein, F., Egret, D., et al.
2000, [A&AS](#), 143, 9
- Zari, E., Hashemi, H., Brown, A. G. A.,
Jardine, K., & de Zeeuw, P. T. 2018, [A&A](#),
[620, A172](#)
- Zari, E., Hashemi, H., Brown, A. G. A.,
Jardine, K., & de Zeeuw, P. T. 2018, [A&A](#),
[620, A172](#)

Table 2. Young, Age-dated, and Age-dateable Stars Within the Nearest Few Kiloparsecs (v0.5 of the CDIPS Target List).

| Parameter | Example Value | Description |
|-------------------|---|--|
| source_id | 1709456705329541504 | Gaia DR2 source identifier. |
| ra | 247.826 | Gaia DR2 right ascension [deg]. |
| dec | 79.789 | Gaia DR2 declination [deg]. |
| parallax | 35.345 | Gaia DR2 parallax [mas]. |
| parallax_error | 0.028 | Gaia DR2 parallax uncertainty [mas]. |
| pmra | 94.884 | Gaia DR2 proper motion $\mu_\alpha \cos \delta$ [mas yr $^{-1}$]. |
| pmdec | -86.971 | Gaia DR2 proper motion μ_δ [mas yr $^{-1}$]. |
| phot_g_mean_mag | 6.85 | Gaia DR2 G magnitude. |
| phot_bp_mean_mag | 6.409 | Gaia DR2 G_{BP} magnitude. |
| phot_rp_mean_mag | 7.189 | Gaia DR2 G_{RP} magnitude. |
| cluster | Uma,IR_excess,NASAExoArchive_ps_20210506 | Comma-separated cluster or group name. |
| age | nan,nan,9.48 | Comma-separated logarithm (base-10) of reported ^a age in years. |
| mean_age | 9.48 | Mean (ignoring NaNs) of age column. |
| reference_id | Ujjwal2020,CottenSong2016,NASAExoArchive_ps_20210506 | Comma-separated provenance of group membership. |
| reference_bibcode | 2020AJ....159..166U,2016ApJS..225...15C,2013PASP..125..989A | ADS bibcode corresponding to reference_id. |

NOTE— Table 2 is published in its entirety in a machine-readable format. This table is a concatenation of the studies listed in Table 3. One entry is shown for guidance regarding form and content. In this particular example, the star has a cold Jupiter on a 16 year orbit, HD 150706b (Boisse et al. 2012). An infrared excess has been reported (Cotten & Song 2016), and the star was identified by Ujjwal et al. (2020) as a candidate UMa moving group member (≈ 400 Myr; Mann et al. 2020). The star’s RV activity and TESS rotation period corroborate its youth.

APPENDIX

A. YOUNG, AGE-DATED, AND AGE-DATEABLE STAR COMPILATION

The v0.5 CDIPS target catalog (Table 2) includes some important updates from previous versions. As in Bouma et al. (2019), we collected membership information for young, age-dated, or age-dateable stars from across the literature. Table 3 gives a list of the sources included, and some brief summary statistics.

The first major important change is that the extent of analyses performed on the Gaia data at the time of our compilation was wide and deep enough that we opted to neglect pre-Gaia analyses, except in cases for which spectroscopically confirmed samples of stars had been collected. The membership lists for instance of Kharchenko et al. (2013) and Dias et al. (2014) (MWSC and DAML) were no longer required, especially given their relatively high field-star contamination rates compared to Gaia-derived membership catalogs.

For any of the catalogs for which Gaia DR2 identifiers were not immediately available, we either followed the spatial (plus proper-motion) crossmatching procedures described in Bouma et al. (2019), or else we pulled the Gaia DR2 source identifiers associated with the catalog from SIMBAD. We consequently opted to drop the ext_catalog_name and dist columns maintained in Bouma et al. (2019), as these were only populated for a small number of stars.

The most crucial parameters of a given star for our purposes are the Gaia DR2 source identifier (source_id), the cluster name (cluster), and the (age). Given the hierarchical nature of many stellar associations, we do not attempt to resolve the cluster names to

Table 3. Provenances of Young and Age-Dateable Stars.

| Reference | N_{Gaia} | N_{Age} | $N_{G_{\text{RP}} < 16}$ |
|--|-------------------|------------------|--------------------------|
| Kounkel et al. (2020) | 987376 | 987376 | 775363 |
| Cantat-Gaudin & Anders (2020) | 433669 | 412671 | 269566 |
| Cantat-Gaudin et al. (2018) | 399654 | 381837 | 246067 |
| Kounkel & Covey (2019) | 288370 | 288370 | 229506 |
| Cantat-Gaudin et al. (2020) | 233369 | 227370 | 183974 |
| Zari et al. (2018) UMS | 86102 | 0 | 86102 |
| Wenger et al. (2000) Y*? | 61432 | 0 | 45076 |
| Zari et al. (2018) PMS | 43719 | 0 | 38435 |
| Gaia Collaboration et al. (2018a) $d > 250 \text{ pc}$ | 35506 | 31182 | 18830 |
| Castro-Ginard et al. (2020) | 33635 | 24834 | 31662 |
| Wenger et al. (2000) Y*O | 28406 | 0 | 16205 |
| Villa Vélez et al. (2018) | 14459 | 14459 | 13866 |
| Cantat-Gaudin et al. (2019) | 11843 | 11843 | 9246 |
| Damiani et al. (2019) PMS | 10839 | 10839 | 9901 |
| Oh et al. (2017) | 10379 | 0 | 10370 |
| Meingast et al. (2021) | 7925 | 7925 | 5878 |
| Wenger et al. (2000) pMS* | 5901 | 0 | 3006 |
| Gaia Collaboration et al. (2018a) $d > 250 \text{ pc}$ | 5378 | 817 | 3968 |
| Kounkel et al. (2018) | 5207 | 3740 | 5207 |
| Ratzenböck et al. (2020) | 4269 | 4269 | 2662 |
| Wenger et al. (2000) TT* | 4022 | 0 | 3344 |
| Damiani et al. (2019) UMS | 3598 | 3598 | 3598 |
| Rizzuto et al. (2017) | 3294 | 3294 | 2757 |
| Akeson et al. (2013) | 3107 | 868 | 3098 |
| Tian (2020) | 1989 | 1989 | 1394 |
| Goldman et al. (2018) | 1844 | 1844 | 1783 |
| Cotten & Song (2016) | 1695 | 0 | 1693 |
| Gagné et al. (2018b) | 1429 | 0 | 1389 |
| Röser & Schilbach (2020) Psc-Eri | 1387 | 1387 | 1107 |
| Röser & Schilbach (2020) Pleiades | 1245 | 1245 | 1019 |
| Wenger et al. (2000) TT? | 1198 | 0 | 853 |
| Gagné & Faherty (2018) | 914 | 0 | 913 |
| Pavlidou et al. (2021) | 913 | 913 | 504 |
| Gagné et al. (2018a) | 692 | 0 | 692 |
| Ujjwal et al. (2020) | 563 | 0 | 563 |
| Gagné et al. (2020) | 566 | 566 | 351 |
| Esplin & Luhman (2019) | 377 | 443 | 296 |
| Roccatagliata et al. (2020) | 283 | 283 | 232 |
| Meingast & Alves (2019) | 238 | 238 | 238 |
| Fürnkranz et al. (2019) Coma-Ber | 214 | 214 | 213 |
| Fürnkranz et al. (2019) Neighbor Group | 177 | 177 | 167 |
| Kraus et al. (2014) | 145 | 145 | 145 |

NOTE—Table 3 describes the provenances for the young and age-dateable stars in Table 2. N_{Gaia} : number of Gaia stars we parsed from the literature source. N_{Age} : number of stars in the literature source with ages reported. $N_{G_{\text{RP}} < 16}$: number of Gaia stars we parsed from the literature source with either $G_{\text{RP}} < 16$, or a parallax S/N exceeding 5 and a distance closer than 100 pc. The latter criterion included a few hundred white dwarfs that would have otherwise been neglected. Some studies appear multiple times when multiple tables from the analysis were included in the concatenation.

a single unique string. The Orion complex for instance, can be divided into almost one hundred kinematic subgroups (Kounkel et al. 2018). Similar complexity applies to the problem of determining homogeneous ages, which we do not attempt to resolve. Instead, we simply merged the cluster names and ages reported by various authors together.

This means that our “age” column can be null, for cases in which the original authors did not report an age, and a reference literature age was not readily available. Nonetheless, since we do generally prefer stars with known ages, we made a few additional efforts to populate this column. When available, the age provenance is from the original analysis of the cluster. However, in a few cases we adopted other ages when the string-based crossmatches on the “cluster” name was straightforward. In particular, we used the ages determined by Cantat-Gaudin et al. (2020) to assign ages to the catalogs from Gaia Collaboration et al. (2018a), Cantat-Gaudin et al. (2018), Castro-Ginard et al. (2020), and Cantat-Gaudin & Anders (2020).

The catalogs we included for which ages were not immediately available were those of Cotten & Song (2016), Oh et al. (2017), Zari et al. (2018), Gagné et al. (2018b), Gagné et al. (2018a), Gagné & Faherty (2018), and Ujjwal et al. (2020). While in principle the moving group members discussed by Gagné et al. (2018b,a); Gagné & Faherty (2018) and Ujjwal et al. (2020) have easily associated ages, our SIMBAD cross-matching lost the moving group association from those studies, which should therefore be recovered tools such as BANYAN Σ .² We also included the SIMBAD object identifiers TT*, Y*O,Y*?, TT?, and pMS*. Finally, we also included every star in the NASA Exoplanet Archive ps table that had a Gaia identifier available (Akeson et al. 2013). If the age had finite uncertainties, we also included it, since stellar ages determined through the combination of isochrone-fitting and transit-derived stellar densities typically have higher precision than from isochrones alone.

The technical manipulations for the merging, cleaning, and joining were performed using pandas (McKinney 2010). The eventual crossmatch (using the Gaia DR2 source_id) against the Gaia DR2 archive was performed asynchronously on the Gaia archive website³.

B. KINEMATIC SELECTION OF δ LYR CLUSTER MEMBERS

Figure 5 shows members of the δ Lyr cluster reported by Kounkel & Covey (2019) to be in the group. Galactic positions are determined and plotted only for stars with parallax signal-to-noise exceeding 20. The location of the Sun is shown on the plots. The non-uniform “clumps” might be an artifact of the data processing steps performed by Kounkel & Covey (2019). We therefore only consider stars in the immediate kinematic group around Kepler 1627. The tangential velocities relative to Kepler 1627 are shown in the bottom right panel. These are computed by assuming that every star has the same three-dimensional spatial velocity as Kepler 1627, where we assume a systemic radial velocity of -16.7 ± 0.2 km s⁻¹ based on the reconnaissance spectra obtained by A. Howard on HIRES

² <http://www.exoplanetes.umontreal.ca/banyan/banyansigma.php>

³ <https://gea.esac.esa.int/archive/>

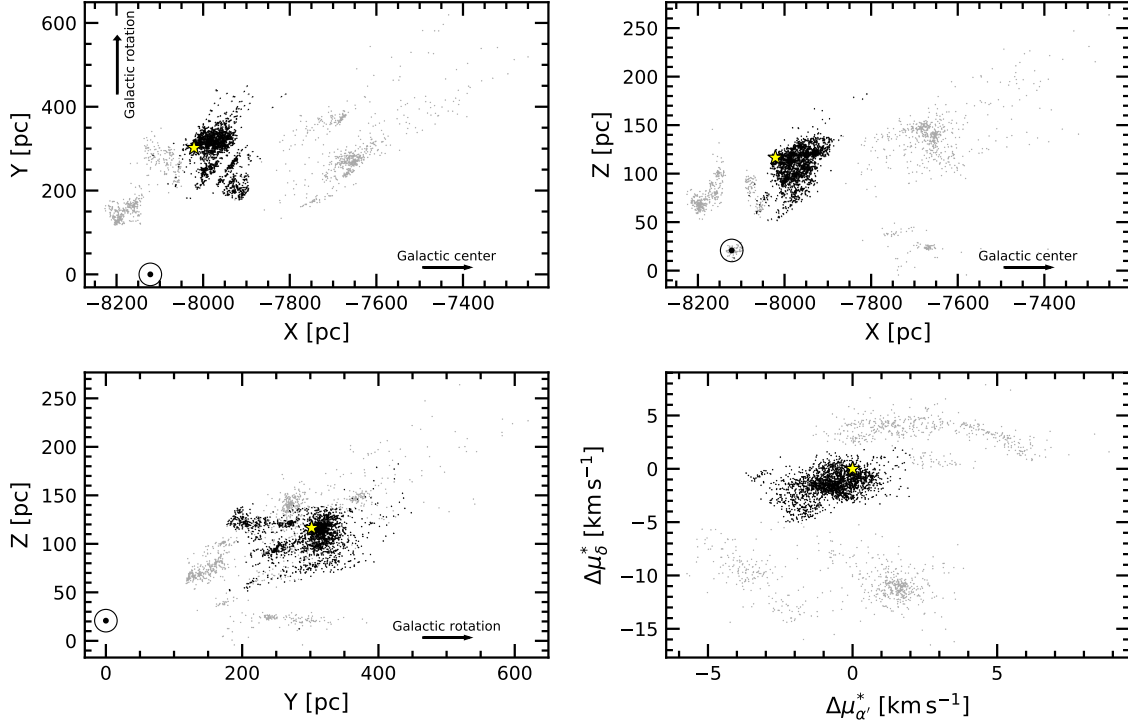


Figure 5. Galactic position and tangential velocities of the δ Lyr cluster (also known as Theia 73 and Stephenson 1). Points are candidate cluster members with $\bar{\omega}/\sigma_{\bar{\omega}} > 20$, reported to be in the group by Kounkel & Covey (2019). We focus on stars in a small region (black points) in the kinematic vicinity of Kepler 1627 (yellow star). The other candidate cluster members (gray points) may or may not share the ages of the selected kinematic group. The location of the Sun is (\odot) is shown.

and D. Latham on TRES. The relevant projection effects are then taken into account, as discussed by *e.g.*, Meingast et al. (2021) and L. Bouma et al (2021, submitted).

C. TRANSIT AND STELLAR VARIABILITY MODEL

C.1. Long Cadence Data

We assumed a quadratic limb-darkening law, with the uninformative prior advocated by CITET Kipping2013.

Our default stellar variability model (RotGPtransit) allows for a RotTerm GP kernel, with a logjitter term to inflate the uncertainties to account for excess white noise. (This results in an inflation of the uncertainties by a factor of about three).

We considered including an additive SHOTerm kernel to account for stochastic noise (RotStochGPtransit). This didn't seem to affect the results much, so we opted for the simpler model.

Figure ?? shows X, Y, Z. The residuals during the transit may hint at some small degree of unfitted signal – in the sense that the observations are systematically high in the first half of transit, and low in the second half. This is the phase of maximal scatter during each orbital period (TODO: in vs out of transit scatter). The amplitude of the anomaly is ≈ 30 ppm.

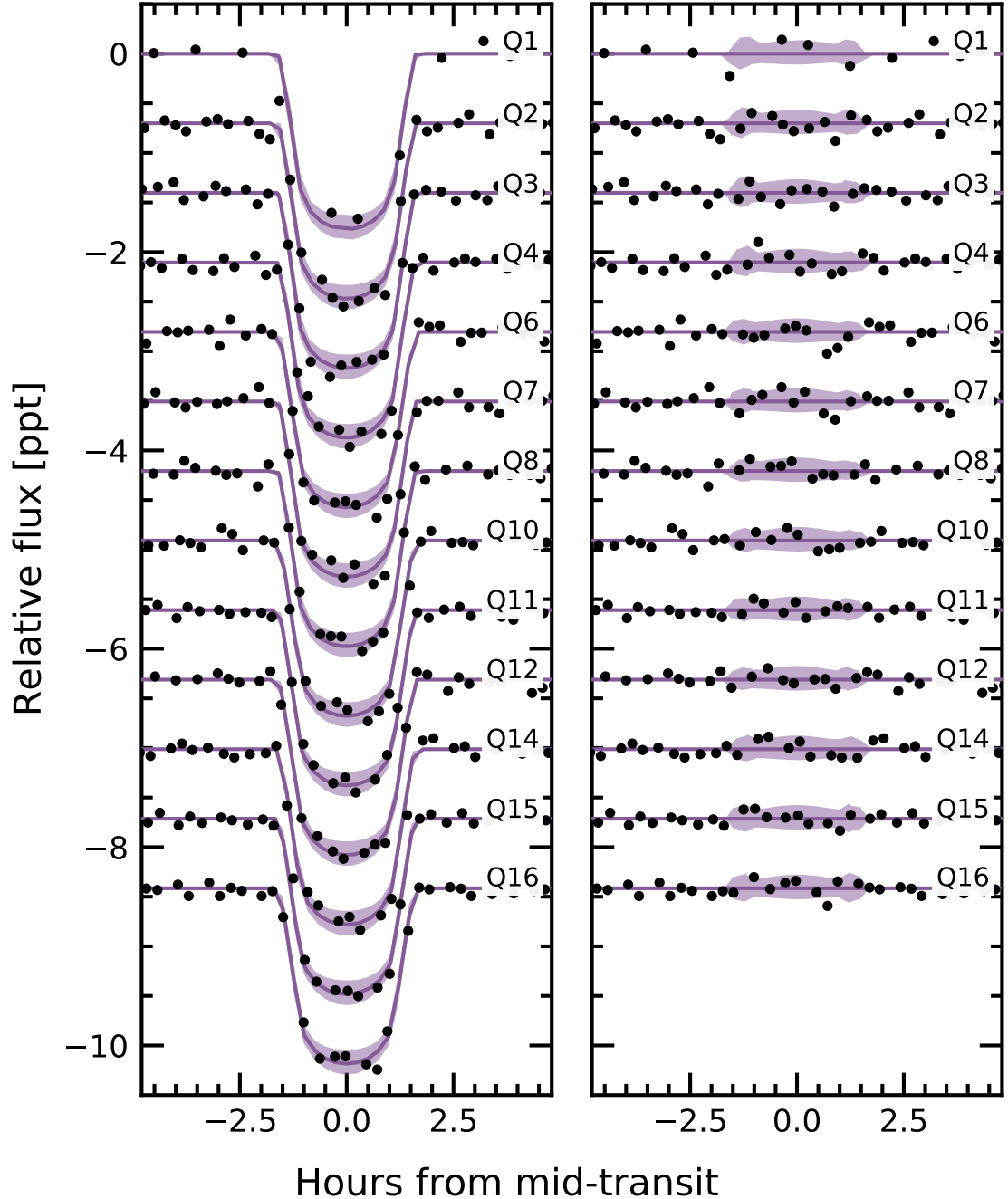


Figure 6. Transit model residuals through time. *Left:* Phase-folded transit of Kepler 1627b, with stellar variability removed, binned by Kepler quarter. Black points are binned to 20 minute intervals. The $1-\sigma$ model uncertainties and the maximum *a posteriori* model are shown as the faint purple band, and the dark purple line. *Right:* As on the left, with the transit removed. Quarters 6 and 7 show a consistent deviation in the second half of the transit.

To explore the origin of the anomaly, we binned the Kepler data over quarters (Figure 6) and years (Figure 7). In Figure 6 Quarter 6 shows the strongest asymmetry out of any of the quarters: a deviation of about 3 ppt from expectation. Quarter 7 shows an anomaly at

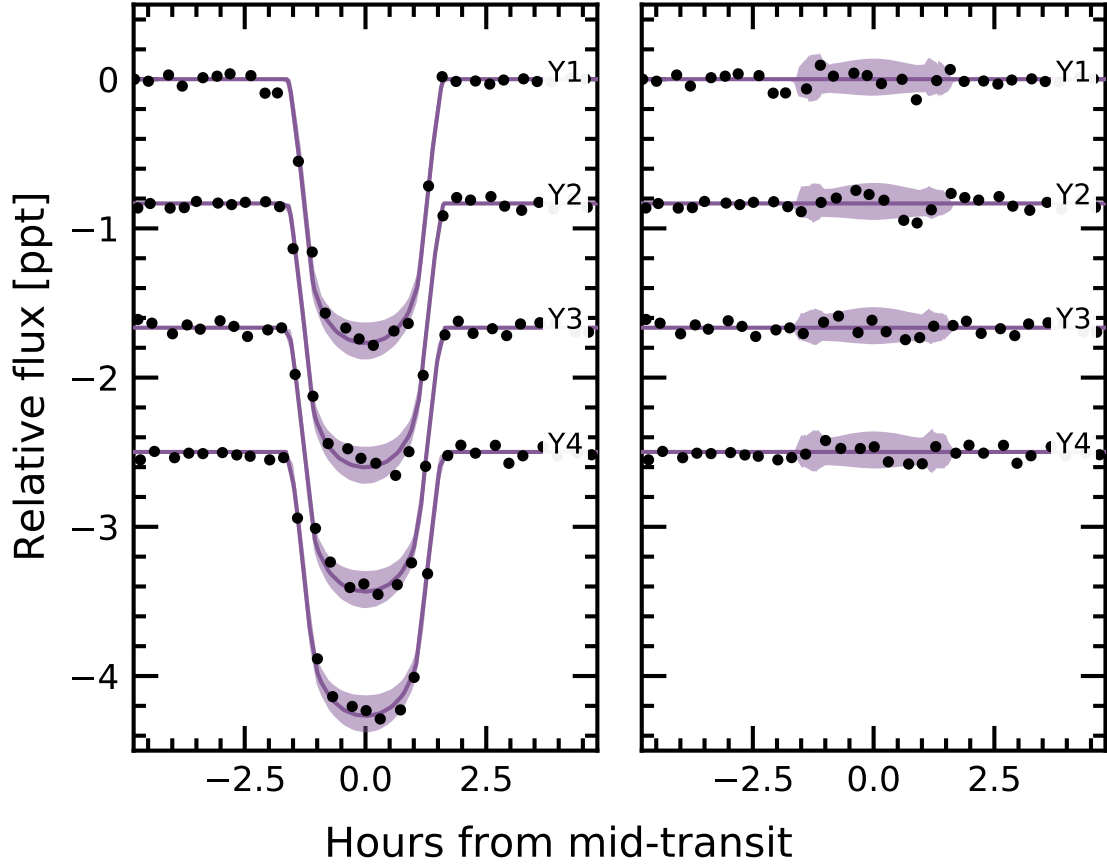


Figure 7. Transit model residuals through time (Part 2). *Left:* Phase-folded transit of Kepler 1627b, with stellar variability removed, binned by year of observation. Points and models are as in Figure 6. *Right:* As on the left, with the transit removed.

roughly the same transit phase. Year 2 correspondingly shows the strongest anomaly out of any year in Figure 7.

We considered three possible explanations for the anomaly: gravity darkening, transit timing variations, and spot-crossing events.

Gravity darkening (e.g., CITE Masuda 2015) is based on the premise that the rapidly rotating star becomes oblate, and brighter near the poles than the equator. The fractional shape change due to gravity darkening is on the order of $(P_{\text{break}}/P_{\text{rot}})^2$, for P_{break} the break-up rotation period, and P_{rot} the rotation period. Using the parameters from Table 1, this yields an expected 1.6% distortion of the ≈ 1.8 ppt transit depth: *i.e.*, an absolute deviation of ≈ 3 ppm. This is smaller than the observed anomaly by an order of magnitude, and therefore seems unlikely.

The scenario of transit timing variations (TTVs) producing the asymmetry seems unlikely, since the analysis by Holczer et al. (2016) implies that any such variations in Kepler 1627 need to be less than of order minutes. Figures 6 and 7 also provide little evidence in support of this possibility.

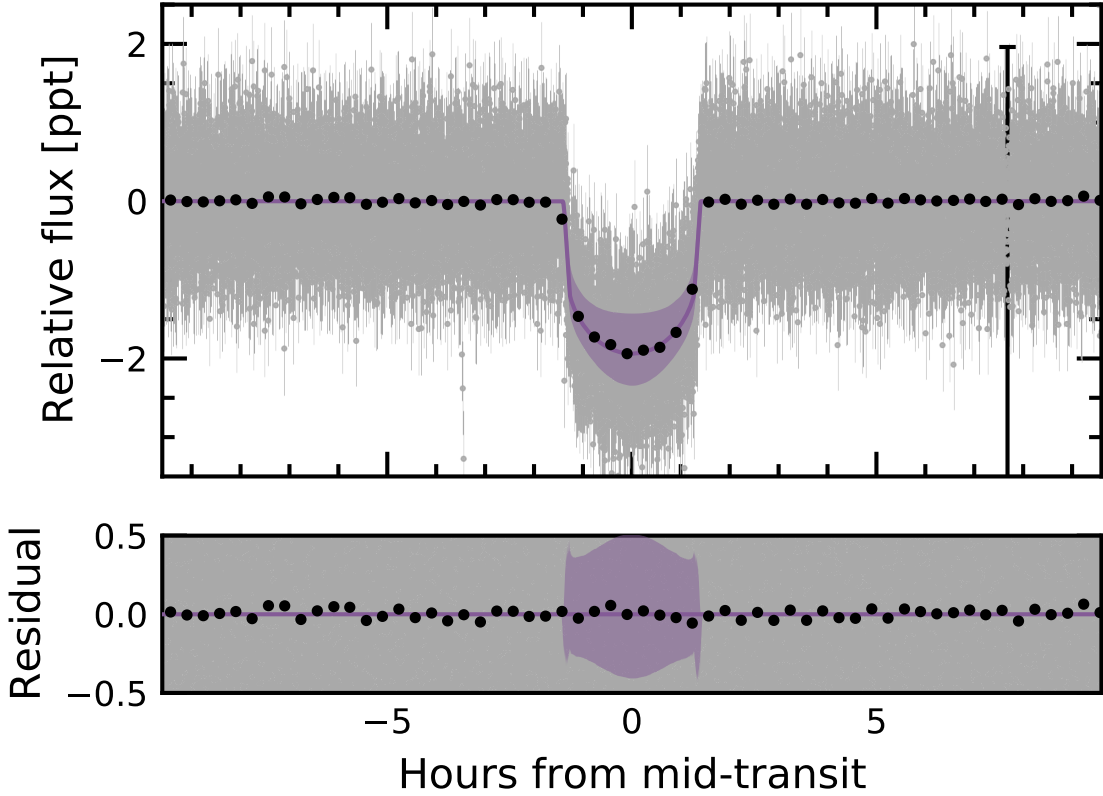


Figure 8. Phase-folded short cadence transit of Kepler 1627 Ab. The precision with which the impact parameter can be measured is higher than from the long cadence data.

The final possibility is that of starspot crossings. Given the high expected spot-covering fractions for young stars (*e.g.*, Morris 2020, Plavchan et al. 2020), Kepler 1627Ab may cross spot groups on the stellar surface in projection. Spot-crossing anomalies often reach amplitudes exceeding 100 ppm (*e.g.*, CITE Dai 2018, maybe Southworth’s recent stuff). For our system, $P_{\text{orb}}/P_{\text{rot}} \approx 2.76$. This means that every 4 transits (and 11 stellar rotations), the planet crosses over roughly the same stellar longitude. Over a given quarter, this could occur at most three times, assuming the spot groups are persistent.

This could provide a plausible path to creating the distorted transit signal, based on the amplitudes involved. However, the typical S/N per Kepler transit is ≈ 8 , making individual spot-crossing unresolved, and this scenario challenging to test. *A priori*, one would also expect the spot-crossing events to not have a preferred orbital phase, so that they would average out over the ≈ 200 Kepler transits. Nonetheless, given the available data, it is our best explanation for what we believe is real additional photometric scatter observed during the transits.

C.2. Short Cadence Data

Figure 8 shows the result from analyzing 100 days of short cadence (1-minute) data acquired during Quarter 15.

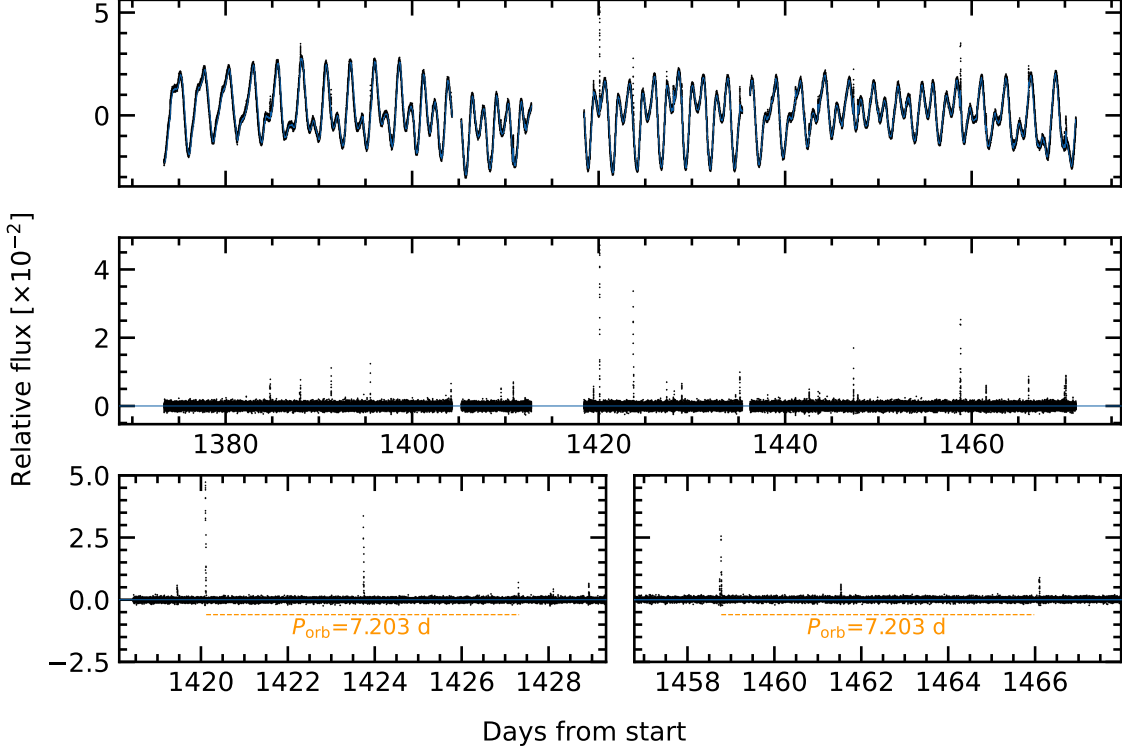


Figure 9. Flares in Kepler 1627. *Top:* The full short-cadence Kepler dataset, acquired at 1-minute sampling (black points) is shown with a stellar variability model (blue line). *Middle:* Residual after subtracting the stellar variability model. Flares appear as spikes. *Bottom:* Zooms of the brightest, and third-brightest flares. A timing coincidence – that both flares have “successors” approximately one orbital period after the initial event – is emphasized.

D. FLARE ANALYSIS

The 1-minute cadence Kepler observations span 98 days, and cover 24 flares exceeding 0.5% in relative flux. These 24 flares spanned a total of 6.5 hours (\sim 15 minutes per flare). The coincidence is that despite the low flare duty cycle, one orbital period after the brightest flare, a second flare followed. This and a similar event are shown in Figure 9. The timing error is good to a $\approx 0.2\%$ difference from the orbital period, which seems *a priori* unlikely. If we consider flares falling within 2% of the planet’s orbital period after a previous flare, then 4 of the 24 flare events have candidate “successors”.

A brief note on how we cleaned the light curve, and identified the flares. For cleaning, we performed the following iterative detrending procedure.

- Step 1: Build a two-term mixed SHOTerm GP model with quasi-periodic kernels at Prot and $0.5 \times \text{Prot}$. Fit the model to the time, flux, and flux uncertainty.
- Step 2: Select points more than twice the median absolute deviation from the residual, and exclude them from the light curve. Repeat Step 1.
- Step 3: On the residual from Step 2, identify all flares, requiring them to be at least 20 cadences apart, at least 7 median absolute deviations above the median baseline, and lasting at least 2 cadences in duration. Build the mask spanning these times,

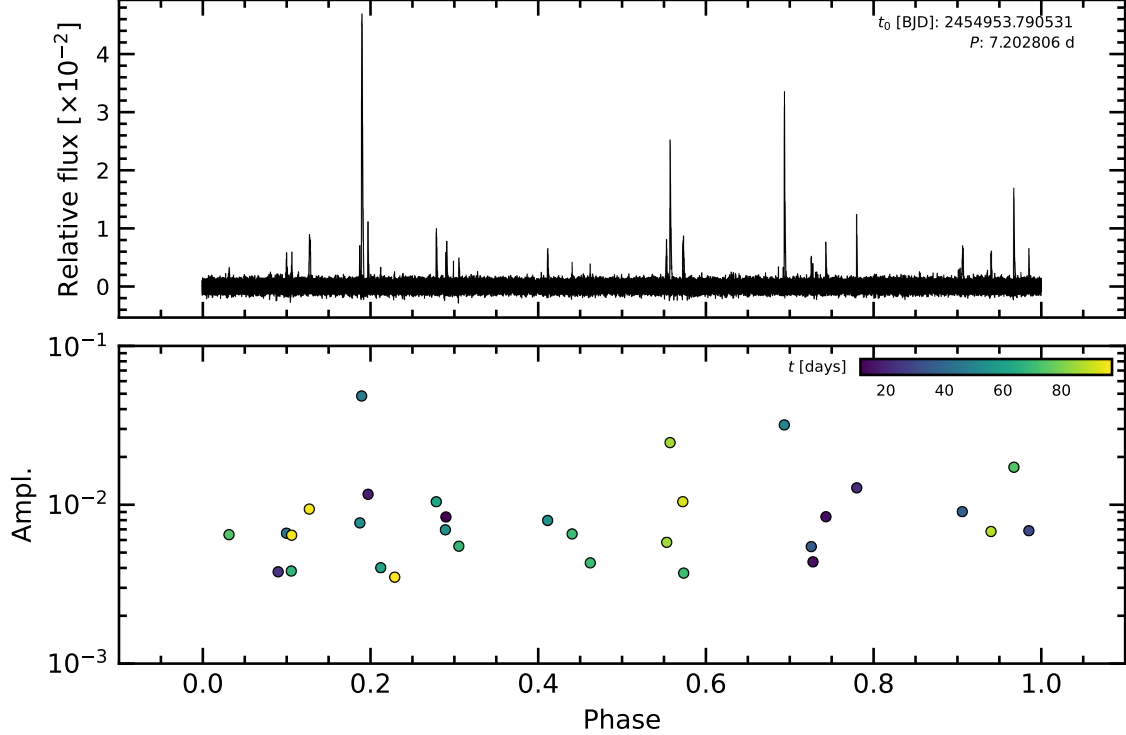


Figure 10. Phase-folded flares in Kepler 1627. *Top:* As in the middle of Figure 9, phase-folded at the planet’s ephemeris. *Bottom:* Fitted flare amplitudes and orbital phases – each point represents one flare. Colors indicate relative time, from the beginning of the 98-day short-cadence Quarter 15 dataset (dark blue) to the end (light yellow). Lower amplitude flares likely exist in the data, and were not examined.

from 5 minutes before each flare begins to 2.5 minutes after the final flare cadence. Repeat Step 1 a final time.

The flares were identified and fitted using ALTAIPONY (CITE CITE). The fitted model is that of CITE XXX, which parametrizes the flare with a start time, a lag time, and an amplitude (CHECK). Figure 10 shows the resulting flares, amplitudes, and phases.

We considered two hypotheses: *i*) the flare arrival times are distributed as a Poisson process, and *ii*) they are better explained as a Poisson process with a periodic mixture component.

TODO: explore! Fit the flare inter-arrival times... [even the 2-separated ones?]

E. COMPANION STAR AND FALSE POSITIVE ASSESSMENT

Our analysis of archival Keck-NIRC2 Kp-band ($2.12\ \mu\text{m}$) imaging revealed the existence of a previously unreported stellar neighbor, unresolved in the Gaia source catalog **FIXME: uncertainties**. The NIRC2 images yield a projected separation $\rho = 0.^{\circ}17$, with $\Delta\text{Kp} = 2.5$. Using the measured Gaia EDR3 parallax for the system, this implies a projected separation of 54 AU. The presence of this star is consistent with the excess noise in the Gaia astrometric time-series (see Section E). Given the low chance of a star imaged within **X.X arcseconds** to be a chance companion along the line of sight, we proceed under the assumption that it is bound, and that the Kepler 1627 system is binary.

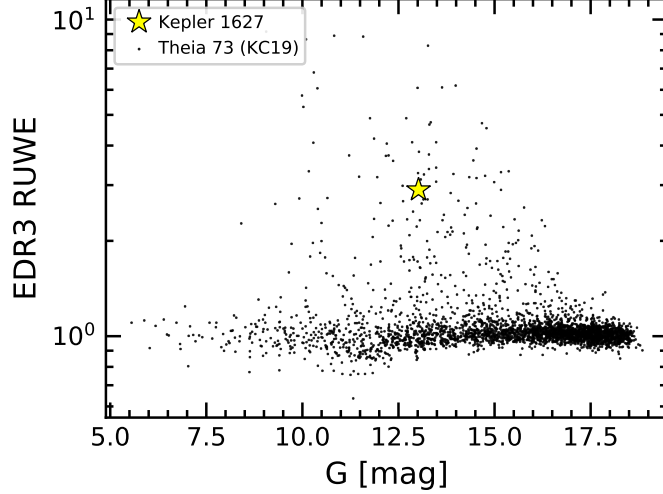


Figure 11. **Gaia EDR3 renormalized unit weight error (RUWE) point estimates for Kepler 1627A and other members of the δ Lyr cluster.** Since other members of the cluster with similar colors have comparable degrees of photometric variability, the high RUWE estimate suggests that Kepler 1627A is a binary.



Figure 12. **Keck NIRC2 AO image of Kepler 1627A and Kepler 1627B.** SCALEBAR DE-NOTES... North is up, East is left.

Unfortunately, we do not have any reliable color information about Kepler 1627B. Based on the tabulation⁴ by Pecaut & Mamajek (2013), the measured NIR-contrast for a main sequence G8V star corresponds to a spectral type for the companion of \approx M2V (M_* \approx $0.44 M_\odot$). However, the companion should have a longer pre-main-sequence contraction phase than the primary, which would imply that this mass is overestimated by \sim 10 to 20%.

⁴ http://www.pas.rochester.edu/~emamajek/EEM_dwarf_UBVIJHK_colors_Teff.txt, version 2021/03/02.

Could the companion be creating a false positive signal? The companion star contributes $\approx 1\%$ of the total flux observed in the Kepler aperture (0.7-2.0% V-band to G-band dmag difference from EEM table; todo is fix using model spectra). The observed transit has a depth of 0.18%. An 18% deep eclipse of the secondary star would therefore be needed to produce a deep enough signal. The shape of the observed signal requires allowed impact parameters to span 0.02 to 0.73 (Table 1); the body transiting the secondary would therefore need to be non-grazing with $R_3/R_2 \approx 0.42$. Assuming a $\approx 0.42R_\odot$ radius of the imaged secondary, this would imply a tertiary stellar radius of $\approx 0.2R_\odot$. This scenario ultimately yields a contradiction, because it would require an ingress and egress phase that each span $\approx 40\%$ of the transit duration (≈ 65 minutes). The actual measured ingress and egress duration is ≈ 15 minutes), $4.4\times$ shorter.

Stellar density implied by transit duration—The duration of the transit ($2.823 \pm 0.057\text{hr}$) and the implied stellar density ($2.31 \pm 0.52\text{ g cm}^{-3}$) could in theory help rule between whether the transiting body orbits the primary or secondary star. Ultimately, our stellar density measurement is not precise enough to render the blend scenario implausible. At 30 Myr, a $0.40M_\odot$ solar-metallicity dwarf is $\approx 26\%$ larger than when it is fully contracted on the main sequence ($0.40R_\odot$ vs. $0.50R_\odot$; CITEALT: Choi et al, MIST grids). The theoretically implied companion density of 3.2 g cm^{-3} is indeed larger than the primary star's density of 1.80 g cm^{-3} (measured through the HIRES reconnaissance spectroscopy). However the stellar density measured from the transit fitting ($2.31 \pm 0.52\text{ g cm}^{-3}$) is only discrepant at the $\approx 2\text{-}\sigma$ level from the M-dwarf blend scenario. It is instead the combination of the flux contrast, transit depth, and ingress duration that rule out this scenario.